LIFE SCIENCES

Egr1 is a 3D matrix–specific mediator of mechanosensitive stem cell lineage commitment

Jieung Baek[1,2], Paola A. Lopez[1,3], Sangmin Lee[4], Taek-Soo Kim[4], Sanjay Kumar[1,2,3,5,6]*, David V. Schaffer[1,2,3,7,8]*

While extracellular matrix (ECM) mechanics strongly regulate stem cell commitment, the field's mechanistic understanding of this phenomenon largely derives from simplified two-dimensional (2D) culture substrates. Here, we found a 3D matrix–specific mechanoresponsive mechanism for neural stem cell (NSC) differentiation. NSC lineage commitment in 3D is maximally stiffness sensitive in the range of 0.1 to 1.2 kPa, a narrower and more brain-mimetic range than we had previously identified in 2D (0.75 to 75 kPa). Transcriptomics revealed stiffness-dependent up-regulation of early growth response 1 (*Egr1*) in 3D but not in 2D. *Egr1* knockdown enhanced neurogenesis in stiff ECMs by driving β-catenin nuclear localization and activity in 3D, but not in 2D. Mechanical modeling and experimental studies under osmotic pressure indicate that stiff 3D ECMs are likely to stimulate *Egr1* via increases in confining stress during cell volumetric growth. To our knowledge, *Egr1* represents the first 3D-specific stem cell mechanoregulatory factor.

INTRODUCTION

Mechanical properties of the cellular microenvironment have increasingly been recognized as important determinants of stem cell behaviors including self-renewal and differentiation (*1*–*4*). In particular, it has widely been accepted that spatial and temporal variations in extracellular matrix (ECM) stiffness modulate cytoskeletal tension and activate mechanotransductive signaling complexes and transcription factors to regulate stem cell behavior (*5*–*8*). In our earlier work, we found that the mechanical stiffness of two-dimensional (2D) ECM substrates regulates neural stem cell (NSC) differentiation, where soft ECMs promote neuronal differentiation and stiff ECMs suppress neurogenesis and elevate glial differentiation (*9*). These effects were mediated by Rho family guanosine triphosphate (GTPase)–regulated cellular contractile forces. In addition, the transcriptional coactivator Yes-associated protein (YAP) was up-regulated on stiff gels and suppressed neurogenesis by binding and sequestering β-catenin, a transcriptional coactivator that would otherwise up-regulate the proneuronal transcription factor NeuroD1 (*10*).

However, most such in-depth mechanistic analysis of how mechanical cues regulate stem cell behaviors involved 2D platforms, which contrast with natural 3D tissue microenvironments (*11*, *12*). On 2D matrices, cell spreading and adhesion are polarized and are unlimited by physical confinement, and cells sense ECM stiffness by exerting inward traction forces (*13*, *14*). In contrast, cell spreading, migration, and growth are confined within 3D matrices, and mechanotransduction can thus also be influenced by other physical factors including the mechanical resistance of the surrounding ECM associated with compression (*15*–*17*) and degradability (*18*–*20*). Furthermore, in many 3D contexts, mechanotransduction and force generation occur through focal adhesion–independent mechanisms (*20*–*22*). For example, cells can migrate in confined 3D matrices in the absence of integrin-mediated adhesions, with cell-ECM forces transmitted through friction (*21*). In addition, neural progenitor cell stemness in 3D matrices may be maintained through matrix remodeling–mediated cell-cell contact in the absence of integrin binding–associated cytoskeletal tension generation (*20*). Last, despite these advances in investigating 3D mechanoregulation, it is not well understood how mechanical inputs ultimately transcriptionally activate target genes that modulate stem cell fate in either 3D or 2D.

In this study, we investigated whether and how NSCs alter their fate choice in response to stiffness in 3D microenvironments. Using engineered hyaluronic acid (HA)–dibenzocyclooctyne (DBCO) hydrogels (*23*), we found that soft gels (0.1 kPa) strongly promoted neurogenesis, and stiff gels (1.2 kPa) suppressed neurogenesis, in a stiffness range that is far narrower than we previously found to regulate NSC fate in 2D (*9*, *10*) and corresponds more closely to the stiffness of adult brain tissue (*24*–*26*). In addition, RNA sequencing (RNA-seq) revealed that the immediate early gene, early growth response 1 (*Egr1*) (*27*–*29*), which encodes early growth response protein 1 (EGR1), was highly up-regulated on stiff versus soft gels, in contrast to 2D gels where its expression was negligible. Furthermore, *Egr1* knockdown (KD) rescued neurogenesis in stiff gels by reversing its suppression of β-catenin signaling. Last, a substantial drop in *Egr1* expression with osmotic manipulation of cell volume supports the idea that ECM confining stress during cell volumetric growth in 3D matrices may contribute to 3D stiffness dependence of *Egr1* expression. In sum, this work implicates *Egr1* as, to our knowledge, the first 3D matrix–specific mechanosensitive regulator of stem cell lineage commitment.

RESULTS

NSC lineage commitment in 3D gel is more mechanosensitive than in 2D gels

To investigate whether the lineage commitment of NSCs within 3D matrices is mechanosensitive, we synthesized a series of HA hydrogels

[1]Department of Bioengineering, University of California, Berkeley, Berkeley, CA 94720, USA. [2]Department of Chemical and Biomolecular Engineering, University of California, Berkeley, Berkeley, CA 94720, USA. [3]UC Berkeley–UC San Francisco Graduate Program in Bioengineering, Berkeley, CA 94720, USA. [4]Department of Mechanical Engineering, KAIST, 291 Daehak-ro, Yuseong-gu, Daejeon 34141, Republic of Korea. [5]Department of Bioengineering and Therapeutic Sciences, University of California, San Francisco, San Francisco, CA 94158, USA. [6]Biological Systems and Engineering Division, Lawrence Berkeley National Laboratory, Berkeley, CA 94720, USA. [7]Molecular Biophysics and Integrated Bioimaging Division, Lawrence Berkeley National Laboratory, Berkeley, CA 94720, USA. [8]Helen Wills Neuroscience Institute, Berkeley, CA 94720, USA.
*Corresponding author. Email: skumar@berkeley.edu (S.K.); schaffer@berkeley.edu (D.V.S.)

in which HA functionalized with DBCO (HA-DBCO) was cross-linked with polyoxyethylene bis(azide) based on strain-promoted alkyne-azide cycloaddition (SPAAC) click chemistry (*23*). We engineered these hydrogels to range in stiffness from 0.1 to 1.2 kPa, which corresponds to the reported elastic modulus of native brain tissue (Fig. 1A and figs. S1, A to F, and S2, A and B) (*24*–*26*). To assess the role of integrin ligation, we generated gels that either lacked or included pendant, azide-conjugated RGD peptides [K(N_3)GSGRGDSPG], hereafter referred to as RGD^- and RGD^+ gels, respectively. RGD conjugation did not significantly alter elastic modulus within our working azide: HA monomer range (0.02 to 0.04).

We next investigated how NSC lineage commitment was affected by matrix mechanics and RGD status. NSCs were encapsulated and cultured in differentiation medium (*9*) that induces a mix of neuronal and glial differentiation for 7 days, fixed, and stained for neuronal (neuron-specific class III β-tubulin, or Tuj1) and astrocytic (glial fibrillary acidic protein, or GFAP) lineage markers. We observed clear stiffness-dependent lineage distribution within this narrow stiffness range, with soft (0.1 kPa) gels strongly promoting neurogenesis and stiff (1.2 kPa) gels suppressing it (Fig. 1, B and C). As anticipated, the opposite trends were observed with respect to astrocytic differentiation. We also noted that the fraction of cells negative for both Tuj1 and GFAP did not differ significantly within 0.1 to 1.2 kPa, indicating that this stiffness range does not notably influence overall cell differentiation (fig. S3). In addition, active caspase 3 levels for each lineage marker–positive cells were low across all the 3D gel conditions throughout the experiment (<4%), ruling out the possibility that the observed differences in lineage commitment were due to selective apoptosis of specific lineage progenitors (fig. S4, A to C). These results differ from our previously reported stiffness-dependent differentiation on 2D gels in two important respects (*9*). First, the range of stiffness sensitivity is much narrower in 3D than in 2D (0.1 to 1.2 kPa for 3D versus 0.75 to 75 kPa for 2D), and accordingly, when NSCs were cultured on the apical 2D surface of these soft and stiff 3D gel formulations, we found no statistically significant variation in neurogenesis (Fig. 1C). Furthermore, only 3D gels showed distinctive morphological differences between soft and stiff gels (Fig. 1B), with a higher number of protrusions in soft gels but smaller and more rounded cellular morphologies in stiff gels for both $Tuj1^+$ and $GFAP^+$ cells. Collectively,

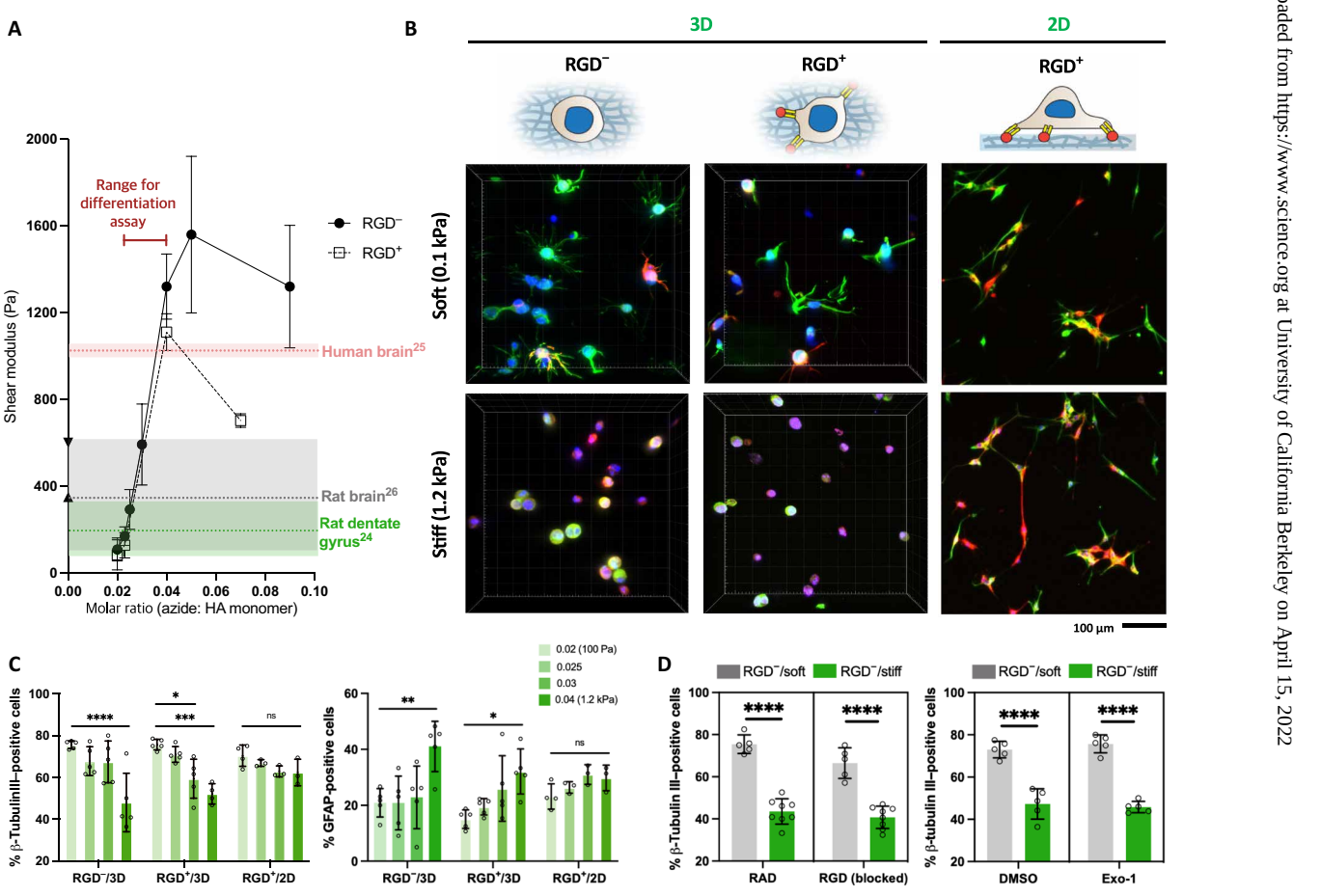

Fig. 1. NSC lineage commitment in 3D gels is more mechanosensitive than on 2D gels between 0.1 and 1.2 kPa. (**A**) Shear elastic moduli of hydrogels controlled by the molar ratio of azides (cross-linker) to HA monomers. (**B**) Representative images of immunostaining for β-tubulin III (green), GFAP (red), and DAPI (blue) in the soft and stiff 3D and 2D hydrogels. Scale bar, 100 μm. (**C**) Quantification of β-tubulin III–positive and GFAP-positive cells in RGD^-/3D, RGD^+/3D, and RGD^+/2D hydrogels. The values 0.02, 0.025, 0.03, and 0.04 represent the molar ratio of azide (cross-linker) to HA monomer. (**D**) Quantification of β-tubulin III–positive cells in the soft (0.1 kPa) and stiff (1.2 kPa) hydrogels with two different condition sets: treatment of RGD sequence–containing peptides and RAD sequence–containing peptides (control) (left) and treatment of Exo-1 and DMSO (control) (right). One-way ANOVA followed by Tukey test $^{****}P < 0.001$, $^{***}P < 0.005$, $^{**}P < 0.01$, $^{*}P < 0.05$. Graphs show means ± SD, $n = 3$ to 5 biological replicates. ns, not significant.

these results suggest that different mechanistic processes may mediate mechanosensitive lineage commitment in 3D versus 2D matrices.

Very similar stiffness-dependent trends in lineage commitment were observed in both RGD$^-$ and RGD$^+$ gels (Fig. 1C), implying the dispensability of RGD-integrin ligation to the overall effect. To assess the possibility that cells in RGD$^-$ gels may be secreting and engaging RGD-containing proteins, we repeated studies in the presence of soluble blocking RGD peptides (and control RAD peptides), which did not appreciably alter the overall result (Fig. 1D and fig. S5A). The results were similarly unaffected by treatment with Exo-1 (fig. S5B), which inhibits secretion of proteins including ECM by limiting vesicular trafficking between the endoplasmic reticulum and Golgi (Fig. 1D) (*30*). Together, these results suggest that the stiffness dependence of NSC lineage commitment is driven by 3D-specific mechanics within the 0.1- to 1.2-kPa stiffness range and that the result is independent of RGD ligand binding.

Egr1 expression is dependent on 3D gel stiffness and regulated by 3D matrix–specific mechanics

To investigate molecular mechanisms underlying mechanosensitive lineage commitment in 3D, we performed unbiased RNA-seq on NSCs encapsulated within the 3D gels under mixed differentiation conditions (Fig. 2A). We harvested mRNA after 12 hours following encapsulation, a time we previously demonstrated NSCs to be maximally primed to respond to stiffness cues in 2D (*10*). We carried out two comparisons (RGD$^+$/stiff versus RGD$^+$/soft and RGD$^-$/stiff versus RGD$^-$/soft) to identify differentially expressed genes (DEGs) between soft and stiff matrices in the presence or absence of RGD. Notably, the heatmap of DEGs for RGD$^+$/stiff versus RGD$^+$/soft showed similar trends as RGD$^-$ gels, i.e., the primary clustering was based on stiffness rather than RGD functionalization (Fig. 2B), reenforcing our earlier data (Fig. 1, B to D) indicating that RGD functionalization is largely dispensable for stiffness-dependent differentiation. Likewise, 83.8% of DEGs from the comparison between RGD$^-$/stiff versus RGD$^-$/soft overlapped with those from the RGD$^+$ gels comparison, and the number of DEGs from RGD$^+$ versus RGD$^-$ was negligible for both soft and stiff gels as compared to that for stiff versus soft. Together, these results indicate that stiffness rather than RGD binding is the more dominant factor regulating the NSC transcriptome at 12 hours in a 3D microenvironment.

Volcano plots of DEGs revealed that compared with soft matrices, stiff matrices uniformly induced higher expression of genes including *Egr1*, Spectrin beta, non-erythrocytic 1 (*Sptbn1*), mitogen-activated protein kinase kinase kinase kinase-4 (*Map4k4*), neural cell adhesion molecule 1 (*Ncam1*), and AT-rich interaction domain 1A (*Arid1a*) (Fig. 2, C and D). The difference was clearest after 12 hours of encapsulation but became more muted after 48 hours, consistent with the idea that NSC lineage is maximally mechanosensitive during a finite time window (fig. S6) (*10*).

We found that *Egr1* was the gene most differentially expressed between stiff and soft matrices, with either the highest (RGD$^+$) or second highest (RGD$^-$) –log$_{10}$ adjusted *P* value. *Egr1* is an immediate early gene (IEG) tightly associated with neuronal activity as well as a variety of higher-order processes such as learning, memory, response to emotional stress, and reward within the central nervous system (*29*, *31*, *32*). In addition, *Egr1* expression has been reported to be rapidly up-regulated by mechanical stimulation in Chinese hamster ovary (CHO) cells (*28*) and is a target of the RhoA (*33*) and extracellular signal-regulated kinase (ERK) (*34*) signaling pathways previously implicated in mechanotransduction. We therefore hypothesized that *Egr1* may be a previously unidentified regulator of NSC mechanosensitive lineage commitment in 3D.

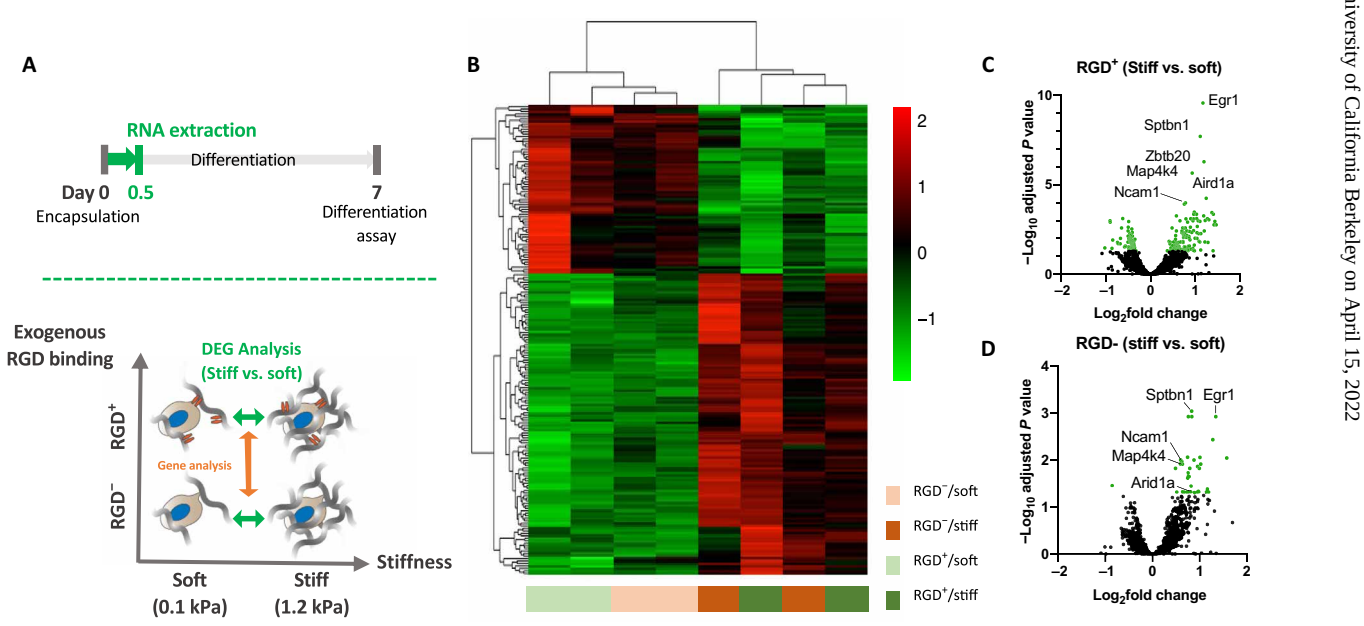

Fig. 2. Regulation of the transcriptome by matrix stiffness in 3D. (**A**) Schematics of experimental timeline (top) and the strategy to compare the overall transcriptome of NSCs based on the exogenous RGD ligand binding and stiffness (bottom). RNAs isolated from the cells embedded in four different hydrogels (RGD$^-$/soft, RGD$^-$/stiff, RGD$^+$/soft, and RGD$^+$/stiff) were used for this analysis. (**B**) A heatmap of the DEGs (from RGD$^+$/stiff versus RGD$^+$/soft comparison) between the four different hydrogels. Dendrograms indicate the clustering of 3D hydrogel conditions (top) and genes (left). Volcano plots of DEGs from stiff versus soft hydrogels with (**C**) and without (**D**) RGD functionalization.

Quantitative reverse transcriptase polymerase chain reaction (qRT-PCR) validation of the RNA-seq results demonstrated that stiffness-dependent *Egr1* expression appeared within 5 hours of encapsulation at levels twofold higher in stiff as compared with soft gels (Fig. 3A). In addition, this level increased for all 3D gels with encapsulation time up to 12 hours. Notably, *Egr1* levels were 70 and 1500 times higher in 3D gels than in corresponding 2D gels cultured in otherwise identical conditions after 5 and 12 hours, respectively, and *Egr1* up-regulation was evident only in 3D. A similar trend was observed irrespective of material platform or RGD incorporation, with negligible *Egr1* expression on 2D gels even when stiffness was raised to 73 kPa (fig. S7A). Then, assessment of the *Egr1* expression levels after inhibition of protein synthesis by treatment of cycloheximide (CHX) was carried out to investigate whether *Egr1* expression is directly mechanosensitive, and thus occurs in the absence of new protein synthesis, or just a downstream marker of NSC lineage commitment. CHX treatment, under conditions that strongly inhibit protein synthesis in NSCs (fig. S7B), did not significantly change *Egr1* expression level or its stiffness dependence in 3D gels (fig. S7C). This result demonstrates that *Egr1* is directly mechanoresponsive and not simply an early marker of the fate commitment. Furthermore, as with lineage commitment, addition of soluble RGD peptides or Exo-1 did not significantly affect the 3D stiffness dependence of *Egr1* (Fig. 3, B and C). To confirm stiffness-dependent expression of *Egr1* at the protein level, we performed Western blotting for EGR1 in the four hydrogels (RGD$^-$/soft, RGD$^-$/stiff, RGD$^+$/soft, and RGD$^+$/stiff). We observed the same trends as in RNA-seq and qRT-PCR (Figs. 2, C and D, and 3A), with markedly higher expression level in stiff gels (Fig. 3D and fig. S7, D and E). EGR1 protein expression was also negligible in 2D gels regardless of material platform and RGD incorporation even at higher stiffness (73 kPa) (fig. S7, F and G). To summarize, *Egr1* expression depended on stiffness only in 3D matrices and independently of RGD binding (Fig. 3E), with a trend that corresponded well with cell differentiation (Fig. 1, B to D).

EGR1 plays a role in the stiffness dependence of NSC lineage commitment only in 3D matrices by regulating β-catenin signaling

To investigate the potential importance of *Egr1* in stiffness-dependent NSC fate commitment in 3D, we depleted *Egr1* with lentivirally delivered short hairpin RNAs (shRNAs) (Fig. 4A). Two shRNAs (shEGR1-1 and shEGR1-2) targeting different regions of *Egr1* mRNA efficiently knocked down EGR1 protein expression compared to cells transduced with a control shRNA (shCtrl) (Fig. 4B). These cells were then differentiated within four different 3D gels (RGD$^-$/soft, RGD$^-$/stiff, RGD$^+$/soft, and RGD$^+$/stiff) under mixed differentiation conditions. Notably, *Egr1* KD rescued neurogenesis in cells in stiff gels compared with shCtrl and naïve cells (Fig. 4, C and D) to levels similar to what we observed for naïve and shCtrl cells in soft matrices, again independent of RGD. Cells in gels with stiffness values greater than 1.2 kPa began to show a reduction in overall differentiation (fig. S8A) after (fig. S8A). [However, these data indicate that *Egr1* KD widens the stiffness range in which maximum neurogenesis (i.e., 70 to 80% on soft gels) is observed.

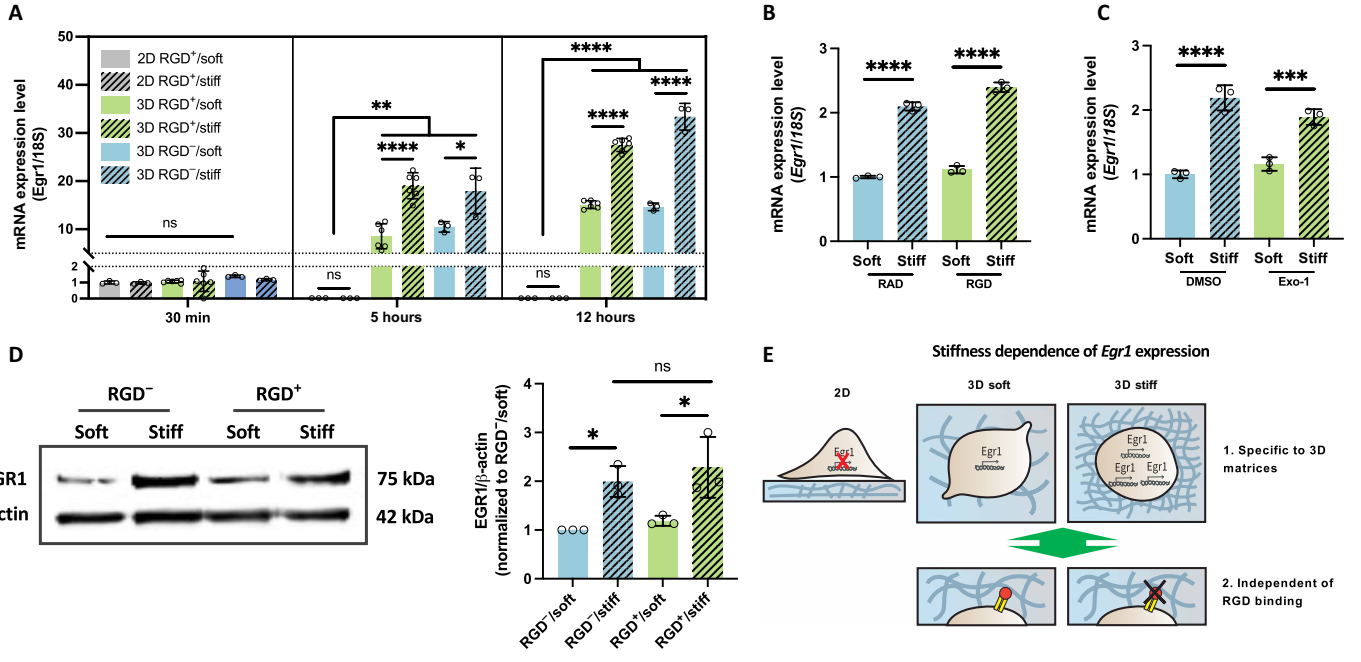

Fig. 3. Matrix stiffness influences *Egr1* mRNA and protein expression in a 3D-specific fashion. (**A**) *Egr1* mRNA expression kinetics during differentiation within bare (RGD$^-$) hydrogels and RGD-ligated (RGD$^+$) 2D and 3D hydrogels. Each level is relative to the expression level on 2D soft gel right after encapsulation (30 min). Hydrogels of 0.1 and 1.2 kPa were used for the soft and stiff conditions, respectively. Expression of mRNA level for *Egr1* in the bare soft and stiff hydrogels with RGD sequence–containing peptides or RAD-containing peptides (control) (**B**) and with DMSO (control) or Exo-1 (**C**). (**D**) Western blot and quantification of EGR1 protein expression in NSCs encapsulated within the four different hydrogels (RGD$^-$/soft, RGD$^-$/stiff, RGD$^+$/soft, and RGD$^+$/stiff) for 24 hours. (**E**) Schematic illustration summarizing the stiffness and RGD dependence of *Egr1* transcription in 3D gels, with stiffness-dependent *Egr1* expression observed only in 3D matrices and independently of RGD-integrin binding. One-way ANOVA followed by Tukey test ****$P < 0.001$, ***$P < 0.005$, **$P < 0.01$, *$P < 0.05$. Graphs show means ± SD.

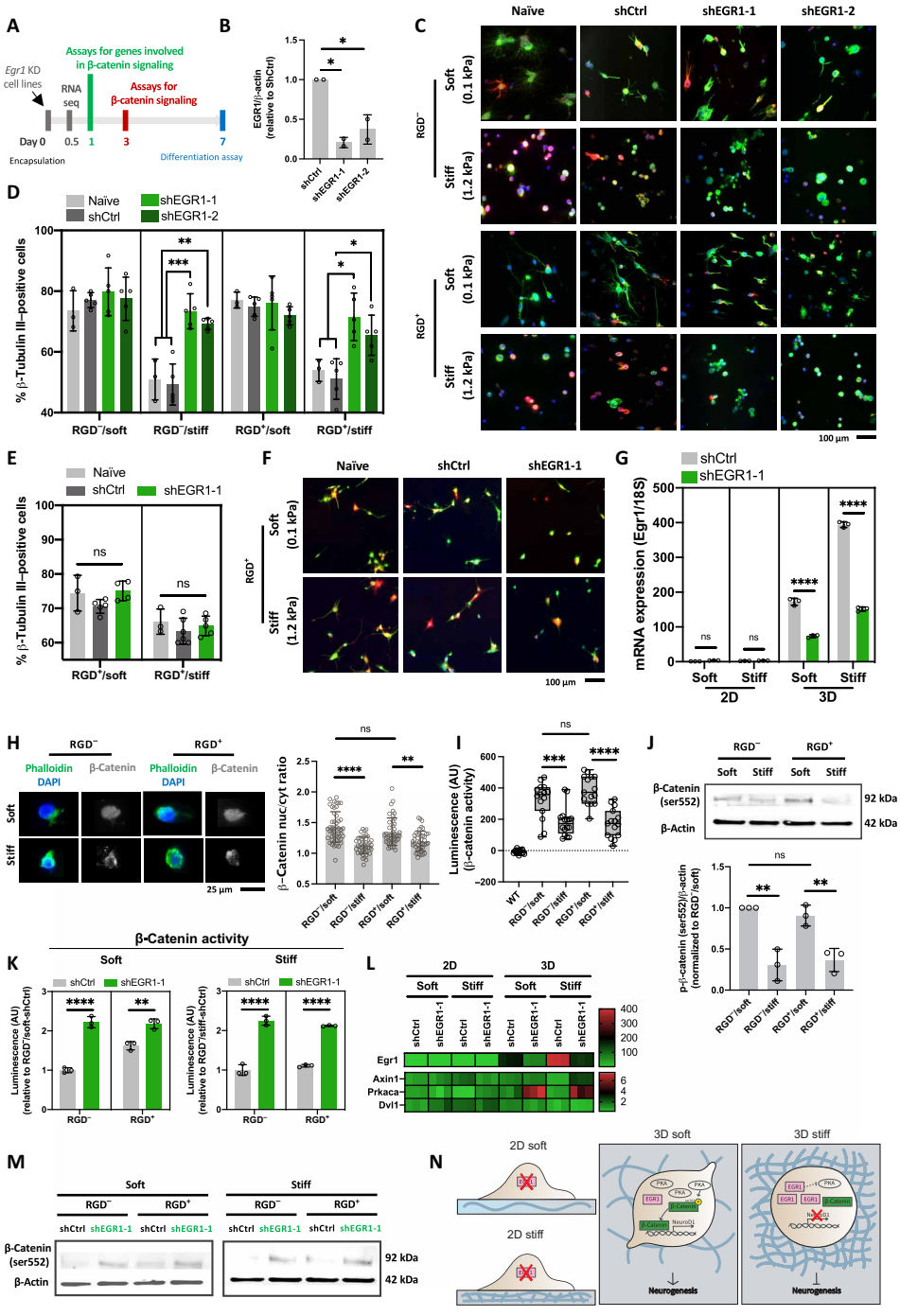

Fig. 4. EGR1 regulates NSC lineage commitment in 3D through β-catenin signaling. (**A**) Experimental timeline for probing β-catenin signaling during lineage commitment. (**B**) EGR1 expression after shRNA KD. $n = 2$. Representative immunofluorescence images of naïve, shCtrl, and *Egr1* KD cell lines stained for β-tubulin III (green), GFAP (red), and DAPI (blue) along with quantification of neurogenesis in 3D (**C** and **D**) and 2D (**E** and **F**) soft (0.1 kPa) and stiff (1.2 kPa) hydrogels. Scale bar, 100 μm. $N = 3$ to 5. (**G**) *Egr1* mRNA levels in shCtrl and shEGR1-1 cell lines in 2D and 3D gels. (**H**) Representative images (left) of immunofluorescence staining for β-catenin (gray), F-actin (green), and DAPI (blue), with corresponding quantification (right) of β-catenin nuclear localization for NSCs encapsulated with RGD$^-$/soft, RGD$^-$/stiff, RGD$^+$/soft, and RGD$^+$/stiff gels. Scale bar, 50 μm. $n > 41$ cells per group. (**I**) Luciferase assay for β-catenin activity in wild-type (WT) and NSC reporter cells embedded in the four different gels. $n = 15$ technical replicates including $n = 3$ biological replicates per each condition. (**J**) Western blotting for active β-catenin (phosphorylated at Ser^{552}) of cells embedded in the four different gels. (**K**) Luciferase assay showing β-catenin activity of shCtrl and shEGR1-1 cells in 3D gels. Values are normalized to shCtrl levels in RGD$^-$ gels within each stiffness. (**L**) mRNA expression level by qPCR of *Egr1* and three different genes (*Axin1*, *Prkaca*, and *Dvl1*) involved in Wnt signaling in 2D and 3D gels. The level for each gene is relative to that of shCtrl on 2D soft gels. $n = 3$ biological replicates. (**M**) Western blotting of active β-catenin (Ser^{552}) of shCtrl and shEGR1-1 cells encapsulated in the four different gels. (**N**) Schematic of the proposed mechanism through which EGR1 acts through β-catenin signaling to regulate stiffness-dependent lineage commitment in 3D. ****$P < 0.001$, ***$P < 0.005$, **$P < 0.01$, *$P < 0.05$.

Consistently, cell lines that overexpress *Egr1* (pMXs-EGR1) (fig. S8B) exhibited lower neurogenesis than control cells (pMXs-GFP) in 3D soft gels (irrespective of RGD status), demonstrating that *Egr1* suppresses neuronal lineage commitment in 3D gels (fig. S8, C to E). No significant *Egr1*-dependent reduction in neurogenesis was observed in stiff gels, confirming the mechanosensitivity of the effect and implying that *Egr1* levels in stiff gels are already sufficiently high to maximally suppress neurogenesis. Thus, *Egr1* is both necessary and sufficient to suppress mechanosensitive neurogenesis in 3D. No significant difference in neurogenesis among naïve, shCtrl, and shEGR1-1 cells was detected for cells on 2D gels (Fig. 4, E and F). This finding is consistent with the very low, stiffness-independent *Egr1* expression seen earlier on 2D gels and further reinforces that *Egr1* does not mediate mechanosensitive lineage commitment on 2D gels (Fig. 4G).

We next asked how *Egr1* regulates neurogenesis in 3D. The Wnt/β-catenin signaling pathway is known to play critical roles in development, differentiation, and maintenance of stemness (*35*–*37*), and our and other groups (*10*, *35*, *38*) have implicated β-catenin signaling in NSC differentiation into neurons. Active, nuclearly localized β-catenin transcriptionally activates *NeuroD1*, a proneuronal transcription factor for NSCs. Intriguingly, it has been reported that EGR1 binding sites are present in the promoters of >15 genes encoding factors in Wnt signaling pathway, indicating a potential link between EGR1 and Wnt signaling in NSC differentiation (*27*).

To investigate whether β-catenin can regulate neurogenesis within 3D matrices, CHIR, a highly potent and specific glycogen synthase kinase-3 (GSK3) inhibitor that potentiates β-catenin activity, was added for 72 hours under differentiation conditions. CHIR treatment enhanced neuronal differentiation and reduced astrocytic differentiation in stiff gels (fig. S9, A to F). We then asked whether β-catenin nuclear localization is regulated by 3D gel stiffness (Fig. 4H) and found that its nuclear/cytoplasmic intensity ratio was higher in both RGD^{-}/soft and RGD^{+}/soft gels compared to the stiff gels, implying that β-catenin more strongly traffics to the nucleus in soft than in stiff gels. We then directly assessed β-catenin–dependent transcription using an established β-catenin–responsive luciferase reporter (*39*), 7xTFP, which we stably introduced into NSCs. We validated this reporter in our system by treating NSCs with CHIR, which resulted in a dose-dependent increase in bioluminescence (fig. S9A). After 72 hours of differentiation in 3D gels, higher luciferase expression was observed in soft gels than in stiff gels (Fig. 4I). Furthermore, Western blotting revealed that the soft gels exhibited higher activated β-catenin (phosphorylated at Ser^{552}) than in stiff gels, confirming stiffness-dependent β-catenin activation at the protein level (Fig. 4J). Together, these observations demonstrate that stiffness-dependent neurogenesis in 3D matrices is regulated by β-catenin signaling. The stiffness-dependent β-catenin activity was not accompanied by differences in levels of YAP, a transcriptional coactivator that has previously been implicated in stiffness-dependent stem cell differentiation (fig. S9G) (*40*–*42*). We recently showed that YAP is up-regulated in NSCs on 2D stiff gels, where it suppresses neurogenesis by binding and sequestering active β-catenin (*10*). In addition, there was no significant difference in the nuclear localization of YAP between soft and stiff 3D gels (fig. S9H). While this result does not definitively rule out a role for YAP in stiffness-dependent *Egr1* expression and neurosuppression, it does suggest that *Egr1* suppresses neurogenesis through a distinct mechanism.

To determine whether EGR1 functionally regulates β-catenin signaling, we made additional shCtrl and shEGR1-1 cell lines that express the 7xTFP β-catenin-responsive luciferase reporter (fig. S9I). *Egr1* suppression greatly enhanced β-catenin activity in all gels, independent of stiffness or RGD functionalization (Fig. 4K). Although *Egr1* suppression increased β-catenin activation in both soft and stiff gels, neurogenesis was not enhanced in soft gels (Fig. 4D), suggesting that β-catenin signaling in 3D soft gels may already be functionally saturated. Furthermore, we performed differentiation assays with shEGR1-1 cells after treatment with MSAB, a selective inhibitor of β-catenin (fig. S10A). Notably, MSAB negated the gains in neurogenesis induced by *Egr1* KD in stiff gels (fig. S10, B and C). This further supports our conclusion that *Egr1* restricts neurogenesis by regulating β-catenin signaling.

To investigate how EGR1 may affect β-catenin signaling in 3D gels, we performed qPCR to quantify mRNA expression levels of three genes that are involved in Wnt signaling and whose promoters harbor EGR1 binding sites (*27*): *Axin1*, Protein kinase cyclic adenosine monophosphate (cAMP)–activated catalytic subunit alpha (*Prkaca*), and Dishevelled segment polarity protein 1 (*Dvl1*) (Fig. 4L). Notably, *Egr1* KD did not reduce *Axin1* levels despite reports that it up-regulates this Wnt signaling repressor and did not significantly alter *Dvl1* levels; however, cells embedded in 3D gels showed 3.9- to 5.5-fold enhancement in the expression of *Prkaca* after *Egr1* KD. *Prkaca* encodes protein kinase A, which has been reported to phosphorylate β-catenin at Ser^{552} and Ser^{675} and thereby promote its transcriptional activity (*43*–*46*). Consistent with this possibility, *Egr1* KD increased the level of Ser^{552}-phosphorylated β-catenin for all the four different gel conditions (Fig. 4M), suggesting that *Egr1* up-regulation in stiff gels suppresses *Prkaca*, thereby decreasing active β-catenin (Ser^{552}). Notably, *Egr1* depletion in 2D did not significantly affect the expression of *Axin1*, *Prkaca*, or *Dvl1* (Fig. 4L), corresponding well with our findings that *Egr1* KD influences NSC fate decisions in 3D but not 2D (Fig. 4, D and E).

Collectively, our results suggest a mechanism by which the stiffness-dependent *Egr1* expression regulates neurogenesis: The abundance of EGR1 in stiff gels may suppress *Prkaca* expression and, thus, β-catenin signaling to reduce neuronal differentiation in 3D matrices (Fig. 4N). In addition, the vanishingly low levels and lack of stiffness-dependent *Egr1* expression in 2D are consistent with weak mechanoregulation in the 0.1-to-1.2 kPa stiffness range (Fig. 1C).

Higher *Egr1* expression in 3D stiff gels is associated with cytoskeletal assembly

We next investigated mechanisms that may link 3D matrix stiffness to *Egr1* expression. We and others (*2*, *9*, *47*) have strongly implicated cytoskeletal assembly and tension in 2D stiffness-dependent stem cell lineage commitment. Cross-sectional imaging in 3D gels showed that cells had more condensed actin structures in stiff than in soft gels (Fig. 5A). Conversely, cells on 2D gels did not exhibit marked differences in actin assembly within the same stiffness range, although cells on gels stiffer than ~2 kPa began to show higher spreading with enhanced actin intensity. These results indicate that the stiffness range of 0.1 to 1.2 kPa is sufficient to drive stiffness-dependent changes in actin cytoskeletal changes in 3D but not 2D. Furthermore, quantification of peak cortex actin intensity after linearization (Fig. 5B) revealed that cells in stiff gels showed higher cortical actin intensity than those in soft gels while exhibiting no notable

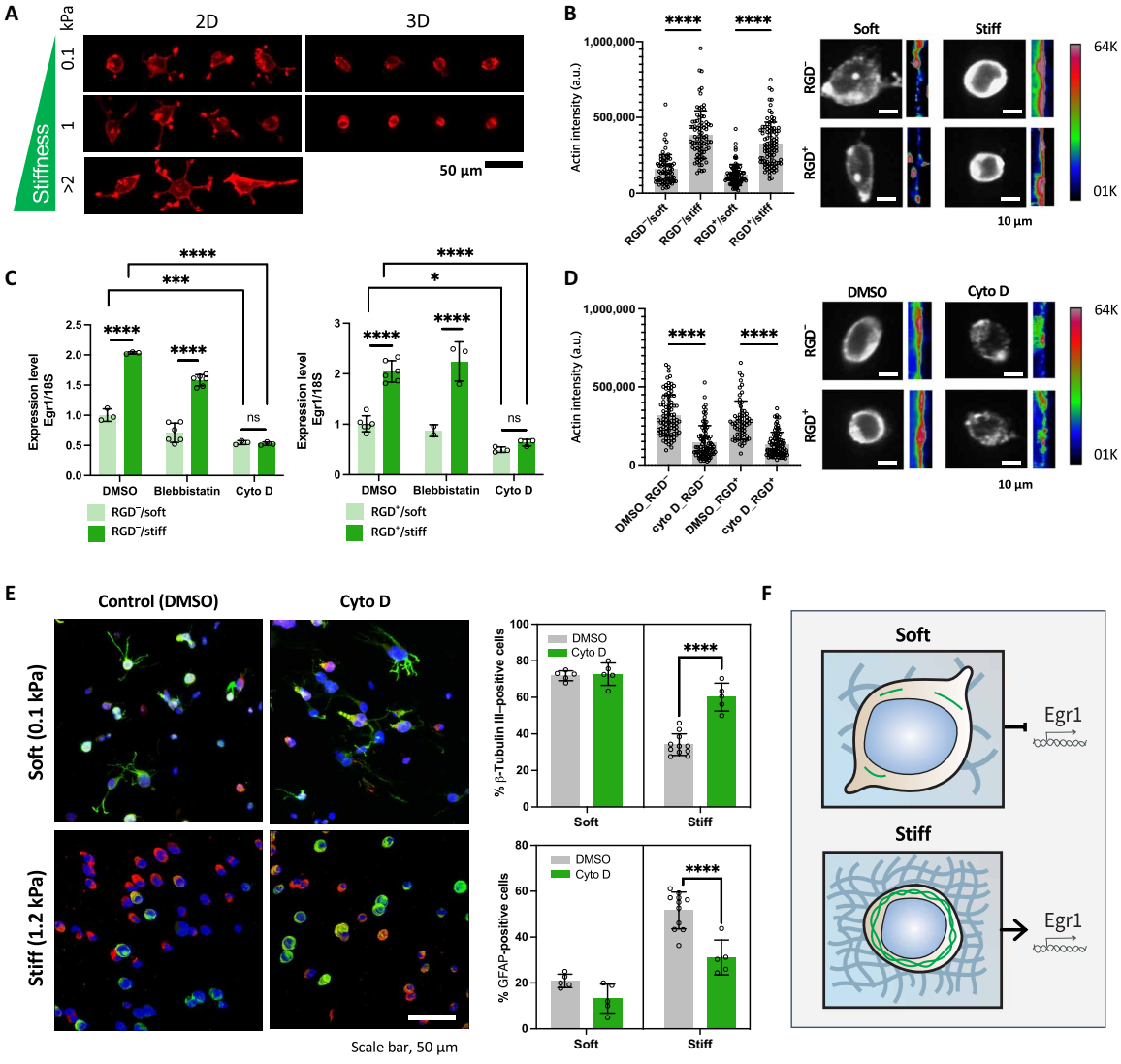

Fig. 5. Actin assembly regulates stiffness dependence of *Egr1* expression in 3D matrices. (**A**) Representative images of rhodamine-phalloidin–stained NSCs differentiated in RGD-functionalized 2D and 3D gels for 4 hours as a function of matrix stiffness (0.1, 1.2, and >2 kPa). Images for 3D gels were obtained after sectioning. Scale bar, 50 μm. (**B**) Quantification of peak cortex actin intensity line scan after background subtraction (left) and representative images of phalloidin-stained cells in the four different 3D gels and color-coded representation of linearized and zoomed-in view of the cortex for each image (right). Images for 3D gels were obtained after sectioning. Scale bar, 10 μm. (**C**) mRNA expression level of *Egr1* after 5 hours of encapsulation with RGD⁻ (left) and RGD⁺ (right) gels after treatment of blebbistatin (1 μM) and cytochalasin D (cyt D, 1 μM) ($n = 3$). DMSO was treated as control. (**D**) Quantification of peak cortex actin intensity line scan (left) and images of phalloidin-stained cells in 3D stiff gels under DMSO- (control) and cyt D–treated conditions (right). (**E**) Representative images of immunostaining for β-tubulin III (green), GFAP (red), and DAPI (blue) and quantification of β-tubulin III– and GFAP-positive cells in RGD⁺ gels after treatment with DMSO (control) and cyt D. Scale bar, 50 μm. (**F**) Schematics showing proposed role of actin assembly in regulation of stiffness-dependent *Egr1* expression in 3D matrices. One-way ANOVA followed by Tukey test ****$P < 0.001$, ***$P < 0.005$, *$P < 0.05$. Graphs show means ± SD. a.u., arbitrary unit.

difference in actin thickness (fig. S11A). To investigate how cytoskeletal tension regulates *Egr1* expression, cells in 3D gels were treated with small-molecule inhibitors against myosin II, actin polymerization, and focal adhesion kinase (FAK) (Fig. 5C and fig. S11, B and C). Inhibition of myosin II and FAK by blebbistatin and PF-573228 (PF), respectively, did not substantially alter the stiffness dependence of *Egr1* expression. Furthermore, cell sphericity, which indicates how spread the cells are in 3D gels, was not significantly changed after the treatment (fig. S11, D and E). However, inhibition of actin polymerization by cytochalasin D (cyt D), which lowered the level of actin intensity but not the thickness (Fig. 5D and fig. S11F), decreased *Egr1* expression and weakened its stiffness dependence. Consistently, disruption of actin polymerization rescued lower neurogenesis in stiff gels (Fig. 5E). Furthermore, treatment of actin stabilizer (jasplakinolide, 25 nM for 3 hours) slightly enhanced the *Egr1* expression level, supporting our conclusion that actin assembly increases *Egr1* expression (fig. S11, G and H).

These results suggest that actin assembly may play a role in stiffness-dependent *Egr1*-mediated neurogenesis that is independent of myosin II-mediated contraction and FAK signaling (Fig. 5F). Furthermore, we investigated whether *Egr1* expression can be regulated by Rho signaling, which is strongly associated with actin

assembly and mechanics (*9*, *48*). Treatment with a selective Rho-associated kinase (ROCK) inhibitor (Y27632) and a Rho kinase activator (Calpeptin) reduced and increased *Egr1* expression levels, respectively (fig. S11, I and J). These results support a mechanism in which increased stiffness enhances Rho/ROCK-dependent actin assembly, leading to increased *Egr1* expression.

Confining stress is a 3D gel–specific mechanism that may contribute to stiffness-dependent actin assembly and *Egr1* expression

Given the 3D-specific role of *Egr1*, we next considered biophysical mechanisms of mechanosensing that may be particularly important in 3D matrices. We reasoned that confining stresses experienced by cells as their volumes expand against the mechanical resistance of the matrix (*15*, *49*) could represent an important regulatory factor operant in 3D but not 2D (Fig. 6A).

We observed that cell volume increases with encapsulation time following induction of differentiation for all the four 3D gels: RGD^-/soft, RGD^-/stiff, RGD^+/soft, and RGD^+/stiff (Fig. 6B). The soft gels showed slightly higher initial volume and more rapid volumetric growth than stiff gels for both RGD^- and RGD^+ conditions. Furthermore, sphericity fell slightly with increasing cell volume in soft gels, but the slope was not steep, with sphericity falling to a relative level of 0.8 to 1 irrespective of stiffness (fig. S12A). This indicates that isotropic volume expansion is more dominant than anisotropic expansion in both soft and stiff 3D gels. This trend was also observed for both soluble RAD peptide– and RGD peptide–treated conditions (fig. S12B), demonstrating that volumetric growth within 3D gels occurs in both soft and stiff gels and is independent of RGD-integrin binding.

We next calculated the confining stress exerted from the surrounding gels to the cell during cell volumetric growth by finite element modeling using ABAQUS 6.14 (Fig. 6C). We defined a model system with a thermally expanding sphere embedded with an elastic cube, where the spheres represent cells that volumetrically grow at a morphological aspect ratio of 1 and a zero stress just after encapsulation (0 hours). Stiff gels showed approximately 8- and 11-times greater stress than soft gels after only 3 hours of encapsulation under RGD^- and RGD^+ conditions, respectively. Furthermore, the time course of increasing stress with encapsulation time corresponds with our observed kinetics for *Egr1* up-regulation (Fig. 3A).

We next investigated whether *Egr1* expression is altered after relieving the effect of ECM confining stress (Fig. 6, C and D). Cell volumetric growth was inhibited by applying an osmotic stress by adding 400-Da polyethylene glycol (PEG 400) to the culture medium. To account for potential ECM-independent effects of osmotic pressure on cells, suspension cells were also incubated under osmotic pressure. Rheometric analysis of the gel under nontreated (Ctrl) and PEG 400–treated (PEG) conditions confirmed that 1.5 weight % (wt %) of PEG does not significantly affect the shear elastic moduli of both soft (0.1 kPa) and stiff (1 kPa) gels (Fig. 6E). However, PEG treatment limited the cell volumetric expansion within the soft gels, even resulting in the volume similar to those in stiff gels for both RGD^- and RGD^+ conditions after 3 hours (Fig. 6F). The restricted cell volume expansion limited the increase in *Egr1* expression level with 3D gel encapsulation time compared with the unrestricted (Ctrl) condition, ultimately leading to significantly different *Egr1* levels between the Ctrl and osmotic pressure (PEG) conditions after 9 hours (Fig. 6G). This volumetric restriction resulted in a marked 8- to 18-fold drop in *Egr1* expression level in a PEG concentration–dependent manner after 3 hours of encapsulation, whereas suspension cells in contrast showed slight increase in *Egr1* expression with PEG 400 concentration (Fig. 6H). This slight *Egr1* increase indicates that a decrease in cell volume, under suspension conditions where cells do not interact with ECM, actually enhances *Egr1* expression. Similar results were observed with 2D gels, where PEG treatment induced a 10- to 20-fold *Egr1* increase (fig. S13, A and B). These results are consistent with the hypothesis that ECM confining stress during cell volumetric growth, a 3D matrix–specific physical factor independent of volumetric growth alone, may play an important role in *Egr1* expression in 3D microenvironments.

Since we previously observed that actin assembly influences *Egr1* expression (Fig. 5C), we next examined whether there is a change in actin architecture after manipulating osmotic pressure. Cells in both soft and stiff 3D gels showed an overall reduction of cortex actin intensity under osmotic pressure (Fig. 6, I and J). This trend correlates well with the lower *Egr1* expression level seen under osmotic pressure (Fig. 6G), suggesting a possible causal link between constrained volumetric growth–mediated regulation of *Egr1* and cytoskeletal assembly.

To determine potential contributions of matrix degradability, we repeated our studies in 3D HA matrices cross-linked with a matrix metalloprotease (MMP)–degradable peptide (highly degradable, KKCGGPQGIWGQGCKK) and a nondegradable peptide control (KKCGDQGIAGFGCKK) (*50*) affixed to the HA-DBCO backbone by terminal azides. Degradable gels showed more extended neurites with slightly enhanced neurogenesis at both soft and stiff conditions as compared with nondegradable control gels (fig. S14). However, degradable stiff gels were not nearly as neurogenic as nondegradable soft 3D gels, demonstrating that differences in matrix degradability do not fully account for our observed stiffness-dependent lineage commitment.

Stiffness-dependent *Egr1* expression is associated with H3K9 trimethylation

In addition to cytoskeletal reorganization, cells could also potentially respond to confining stress through nuclear reorganization. Stiff gels induced a smaller nuclear size than soft gels for both RGD^- and RGD^+ conditions, indicating that nucleus is mechanically influenced by 3D gel stiffness regardless of RGD binding, as we previously observed for actin formation (Fig. 7A). Chromatin architecture, which is regulated in part by enzymatic acetylation and methylation, has recently been reported to exhibit stiffness-dependent accessibility in 3D matrices, with concomitant changes in gene expression (*51*). In particular, demethylation of histone H3 lysine-9 trimethylation (H3K9me3) has been shown to induce Pol II recruitment and increase *Egr1* transcription in cells under force (*28*). It has recently been reported from High-throughput Chromosome Conformation Capture (Hi-C) analysis that H3K9me3 is a strong functional marker for transcriptionally inactive chromosomal regions (*52*). Accordingly, we examined whether H3K9 trimethylation levels are dependent on stiffness under three different gel conditions: RGD-presenting 2D gels, RGD^- 3D gels, and RGD^+ 3D gels (Fig. 7B). 3D but not 2D gels exhibited stiffness-dependent H3K9 methylation, with higher H3K9me3 in soft than in stiff gels. Furthermore, the H3K9 demethylase inhibitor JIB-04 notably reduced *Egr1* expression for all 3D gel conditions (RGD^-/soft, RGD^-/stiff, RGD^+/soft, and RGD^+/stiff) despite an only 1.3-fold increase

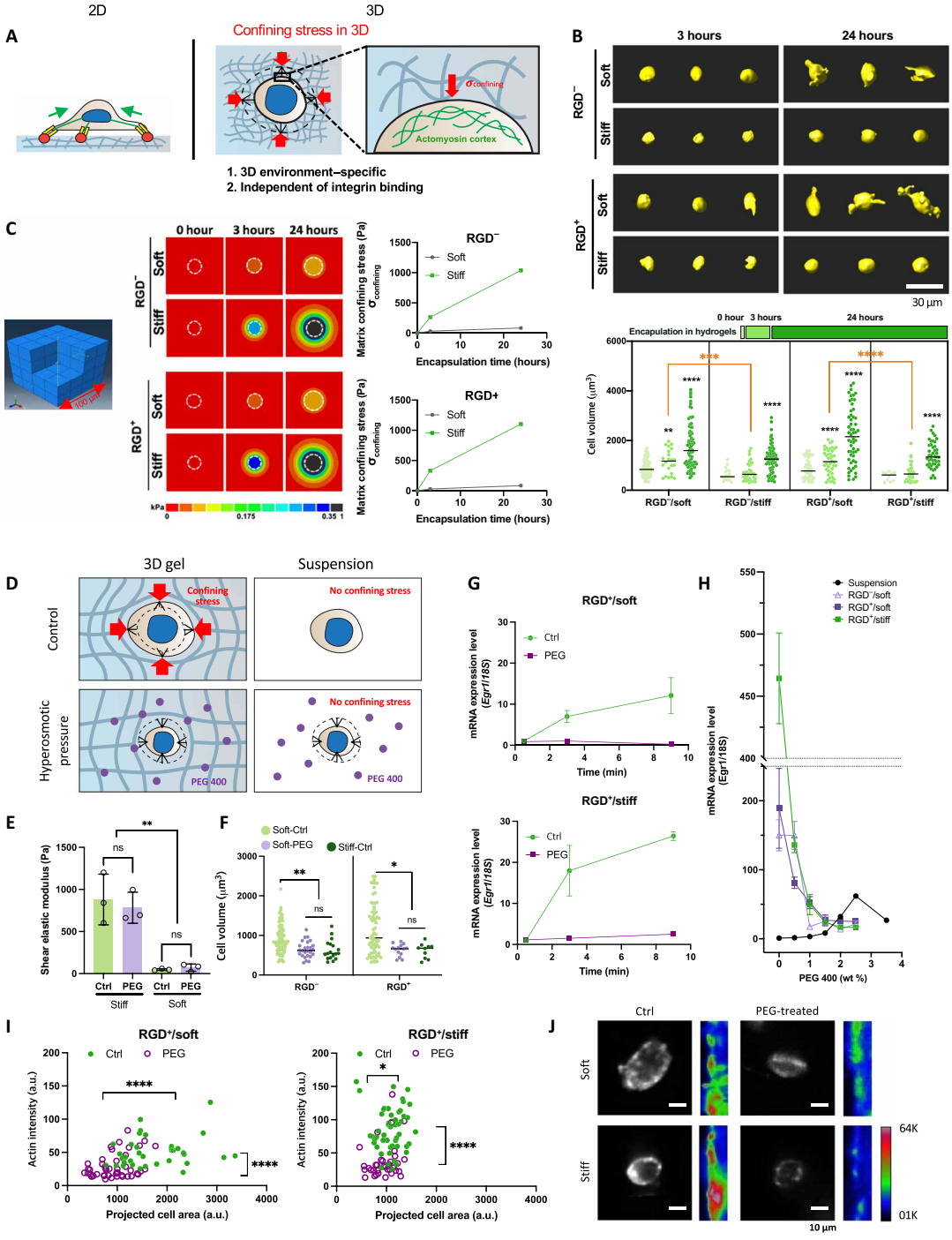

Fig. 6. Regulation of stiffness-dependent *Egr1* expression by confining stress during 3D volumetric growth. (**A**) Schematics illustrating potential role of confining stress as a 3D-specific regulator of *Egr1* expression. (**B**) Representative 3D rendering of NSCs after 3 or 24 hours of encapsulation (top) and cell volumes (bottom). Cells were embedded in RGD$^-$/soft, RGD$^-$/stiff, RGD$^+$/soft, and RGD$^+$/stiff gels; 10 to 77 cells per group. Scale bar, 30 μm. (**C**) ABAQUS simulation to calculate matrix confining stress during cell volumetric growth in the four gel conditions, showing: model system (left), color-coded stress field with the direction of matrix to the cells (center), and quantified stress values with incubation time (right). Close similarities between RGD$^+$ and RGD$^-$ conditions reflect the RGD independence of measured cell volume, an input parameter. White dotted line represents the cell boundary. (**D**) Schematics depicting application of osmotic pressure to the cells in 3D gels to release confining stress during volumetric growth. Dotted line represents the cell size right after encapsulation. (**E**) Shear elastic moduli of RGD$^+$/soft and RGD$^+$/stiff gels incubated under nontreated (Ctrl) and PEG (1.5 wt %)–treated conditions for 3 hours. (**F**) Cell volume in soft gels with and without PEG (1.5 wt %) and stiff gels without PEG (3 hours). (**G**), *Egr1* mRNA expression level changes in RGD$^+$ soft and stiff gels under Ctrl and PEG (1.5 wt %) conditions (30 min, 3 hours, and 9 hours). (**H**) *Egr1* expression as a function of PEG concentration for cells in suspension and in gels. (**I**) Scatter plot of peak cortex actin intensity versus projected cell area of the cells encapsulated in 3D RGD$^+$/soft (left) and RGD$^+$/stiff (right) gels under Ctrl or PEG (1.5 wt %) condition for 3 hours. (**J**) Representative images of phalloidin-stained cells in sectioned RGD$^+$ gels under the Ctrl and PEG conditions and color-coded linearized view of the cortex for each image. Scale bar, 10 μm. ****$P < 0.001$, ***$P < 0.005$, **$P < 0.01$, *$P < 0.05$.

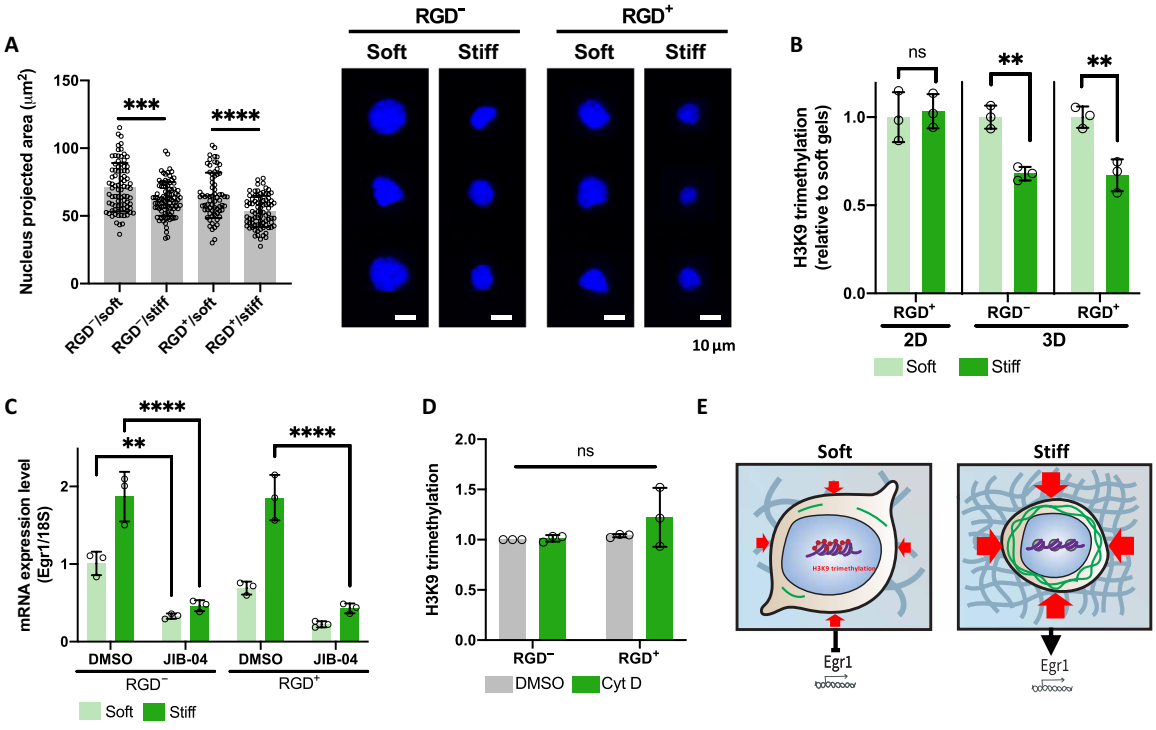

Fig. 7. H3K9 trimethylation is associated with stiffness-dependent *Egr1* expression in 3D matrices. (**A**) Projected area of cell nuclei in the four different 3D gels (RGD$^-$/soft, RGD$^-$/stiff, RGD$^+$/soft, and RGD$^+$/stiff) (left) and corresponding representative images of DAPI-stained cells in the gels after sectioning. $N > 69$ cells were used for each condition. Scale bar, 10 μm. (**B**) Stiffness dependence of H3K9me3 level in 2D and 3D gels ($n = 3$). (**C**) mRNA expression level of *Egr1* in the four different 3D gels after treatment of DMSO (control) and JIB-04 (3 μM) for 3 hours. All values are normalized to values for DMSO-treated RGD$^-$/soft gels ($n = 3$). (**D**) H3K9me3 level of cells in RGD$^-$ and RGD$^+$ stiff gels after treatment of DMSO (control) and cyt D (1 μM). (**E**) Proposed mechanism for regulation of *Egr1* expression by 3D gel stiffness–dependent confining stress via H3K9 trimethylation. One-way ANOVA followed by Tukey test. ****$P < 0.001$, ***$P < 0.005$, **$P < 0.01$. Graphs show means ± SD.

in H3K9me3 levels after JIB-04 treatment (Fig. 7C and fig. S15). Stiffness-dependent *Egr1* expression was also slightly weakened by inhibition of H3K9 demethylase. Although this value was not as significantly altered as with actin assembly inhibition (Fig. 5C), the substantial decrease in *Egr1* expression level for each gel condition indicates that H3K9me3 restricts the transcription of *Egr1* in 3D gels. Given that both actin and H3K9 trimethylation play a role in *Egr1* expression in 3D gels, we investigated whether altered actin assembly and H3K9 trimethylation are directly correlated with each other in a process of regulating stiffness-dependent *Egr1* transcription in 3D gels. H3K9me3 levels did not substantially change after inhibition of actin assembly in either RGD$^-$ or RGD$^+$ stiff gels, indicating that any alterations in cortical actin assembly observed in 3D stiff gels do not significantly influence H3K9 trimethylation (Fig. 7D). Together, our results demonstrate that less trimethylation of H3K9 in stiffer gels may induce higher *Egr1* expression levels compared with soft gels, an effect that could potentially be linked with the stiffness-dependent confining stress (Fig. 7E). While our results are broadly supportive of an epigenetic component to *Egr1*-mediated neurosuppression, a stronger causal case could be made with studies focused on the *Egr1* locus along with more global studies such as chromatin immunoprecipitation followed by sequencing.

DISCUSSION

We investigated whether, and by what mechanism, NSCs exhibit mechanosensitive differentiation in 3D. Using a cross-linked HA-DBCO gel, we observed that ECM stiffness regulates 3D mechanosensitive fate decisions in a narrower and more brain-mimetic stiffness range than 2D. Through unbiased transcriptome analysis, we identified a 3D matrix–specific mechanosensitive regulator, *Egr1*, whose genetic perturbation established its critical role in stiffness-dependent suppression of β-catenin signaling and neuronal differentiation. Furthermore, our results are consistent with the hypothesis that stiff 3D gels suppress neurogenesis because of enhanced confinement stress during volumetric expansion, which modulates actin assembly and increases *Egr1* expression (fig. S16).

While several studies have shown differences in mechanosensitive stem cell behaviors between 2D and 3D microenvironments (*5*, *18*, *19*), little is known about how dimensionality-specific physical factors and their underlying biomolecular mechanisms regulate stem cells. In this study, we identified EGR1 as a key a mechanoresponsive transcriptional factor that regulates stiffness-dependent NSC lineage commitment. *Egr1* exerted functional effects in 3D but not in 2D, where cells exhibited negligible *Egr1* expression. To our knowledge, *Egr1* thus represents the first reported 3D matrix–specific mechanosensitive stem cell regulatory factor. Higher expression of *Egr1* in 3D stiff gels suppressed the expression of *Prkaca* and in the activation of β-catenin signaling, raising the possibility of 3D-specific *Egr1* regulation of β-catenin signaling in numerous other biological processes. (*53*, *54*) For example, *Egr1* is known to regulate the synaptic plasticity and activity of mature neuronal circuits, (*29*, *31*, *32*), and if it is also mechanosensitive in this context, it could modulate neuronal activity in older brain, which is known to soften with aging.

Another intriguing finding was that the stiffness-dependent *Egr1* expression was highly associated with a property specific to 3D matrix–specific mechanics (ECM confining stress), potentially explaining why *Egr1* mediates mechanosensitive lineage commitment only in 3D. Osmotic restriction of cell volumetric growth in stiff 3D gels, which would be expected to reduce confining stress, altered actin cytoarchitecture and attenuated *Egr1* expression. Thus, confining stress appears to increase *Egr1* expression and influence stiffness-dependent lineage commitment through a mechanism that involves altered actin cytoarchitecture.

Unexpectedly, stiffness-dependent NSC transcriptome in general (Fig. 2B) and regulation of *Egr1* expression specifically were observed in both bare gels and gels functionalized with an RGD peptide and occurred even upon inhibiting protein secretion by Exo-1. Of course, these findings do not rule out the possibility that adhesion to RGD motifs, secreted matrix, or the HA backbone itself regulates other important biological functions besides lineage commitment (*55*, *56*). Instead, our model points to the centrality of confining stress in regulating lineage commitment, which is dictated by the mechanical properties of the surrounding matrix and not particular mechanism of adhesion.

Together, our work establishes an *Egr1*-mediated mechanotransduction pathway that controls lineage commitment through mechanisms that are intrinsic to 3D matrices. In the future, it would be fruitful to develop strategies to directly manipulate confining stress independently from stiffness in 3D matrices to more precisely isolate the effect of confining stress on actin assembly, chromatin modification, and *Egr1* expression. It will also be important to more thoroughly identify the molecular mechanisms that link actin assembly, *Egr1* expression, β-catenin, and neurogenic lineage commitment.

MATERIALS AND METHODS

Cell culture and differentiation

Adult rat hippocampal NSCs were derived from adult female Fischer 344 rats (Charles River) as previously described (*57*). The cells were cultured in Dulbecco's modified Eagle's medium/nutrient mixture F-12 (DMEM-F12, Gibco) supplemented with N2 supplement (Life Technologies) and fibroblast growth factor (FGF)–basic (20 ng/ml; Peprotech) on the tissue-culture polystyrene plates coated with poly-ornithine (10 μg/ml, Sigma-Aldrich) and laminin (5 μg/ml, Invitrogen) sequentially. The growth medium for undifferentiated cells was replenished every 2 days. To attain the cells in differentiated state, the cells were cultured in mixed differentiation medium (DMEM-F12 with N2 supplemented with 1 μM retinoic acid and 1% fetal bovine serum) right after being seeded onto gels or encapsulated with gels. The medium was replaced every 2 days during 7 days of differentiation process. Then, the cells were fixed for immunofluorescence imaging.

DBCO functionalization to HA

Before making hydrogels, HA was modified with DBCO. First, carboxylic acid groups of sodium hyaluronate (average molecular weight 75 kDa; Lifecore Biomedical) dissolved in 2-(*N*-morpholino) ethanesulfonic acid (MES) (1 mg/ml) were activated by *N*-(3-dimethylaminopropyl)-*N*′-ethylcarbodiimide (EDC, Sigma-Aldrich) and *N*-hydroxysuccinide (NHS; Sigma-Aldrich) for 1 hour. Then, 0.6 equivalents of DBCO-amine (Sigma-Aldrich) in dimethylsulfoxide (DMSO) were added dropwise to the solution. After 48-hour reaction at room temperature, unreacted starting materials in the mixture were removed by centrifugation with a 10-kDa cutoff concentrator (Millipore), and the remaining reaction mixture was precipitated and washed with cold acetone twice. The precipitate was dissolved in ultrapure water and lyophilized for 2 days. The extent of DBCO functionalization to HA was estimated by 1H nuclear magnetic resonance spectroscopy.

Making HA-DBCO hydrogels

We formed HA-DBCO hydrogels by SPAAC, a bio-orthogonal gelation chemistry. HA-DBCO was dissolved in DMEM/F-12 to a final concentration of 3 w/v %, and poly(ethylene glycol) bisazide (PEG-bisazide; average M_n, 1100; Sigma Aldrich) was added for cross-linking. RGD sequence–containing peptide with azide functionality [K(N_3)GSGRGDSPG, 1 mM, Genscript] was also added to the HA formulation at the same time as necessary. Then, the mixture was incubated for 10 min at 37°C for cross-linking. The amounts of HA-DBCO and PEG-bisazide were varied to obtain the gels with different stiffnesses. The molar ratio of DBCO to HA monomer was controlled to be 0.02, 0.025, 0.03, and 0.04 with constant final HA-DBCO concentration in the hydrogel (3 wt %). For encapsulating the cells within hydrogels, cell suspension was added to the HA-DBCO solution right before adding PEG-bisazide.

Hydrogel characterization

Hydrogel stiffness was characterized by shear rheology via a Physica MCR 301 rheometer (Anton Paar) with an 8-mm parallel plate geometry for $\gamma = 0.5\%$ and $f = 1$ Hz. Frequency was controlled to be between 50 and 1 Hz for the frequency sweep at a constant strain ($\gamma = 0.5\%$), and the modulus saturation curve with time was obtained under oscillation with constant strain ($\gamma = 0.5\%$) and frequency ($f = 1$ Hz). The temperature of the gel solution was controlled ($T = 37$°C) with a Peltier element (Anton Paar), and water was added around the solvent trap to prevent sample dehydration. Elastic modulus maps were also characterized by atomic force microscopy on a Vaeco (Bruker) Catalyst Bioscope instrument. The gel sample was soaked in cell culture medium (DMEM/F-12) at room temperature for all measurements. The deflection sensitivity of each MLCT-Bio cantilever was measured against a glass cover slide, and the spring constant was obtained by thermal tuning. Sneddon indentation model (cone indenting infinite half-space) was used to fit force-indentation curves for calculating elastic moduli.

Immunocytochemistry

Samples were fixed by incubating with 4% paraformaldehyde in phosphate-buffered saline (PBS) for 15 min at room temperature. After thorough washing with PBS, the fixed cells were permeabilized and blocked with Triton X-100 (0.3 %) and bovine serum albumin (3%) in PBS for 35 min at room temperature (RT). Then, the samples were incubated at 4°C for 48 hours with the following primary antibodies: mouse anti-tubulin β3 (1:1000; BioLegend), rabbit anti-GFAP (1:1000; Abcam), rabbit anti-Egr1 (1:1000; Cell Signaling Technology), and rabbit anti–β-catenin (Cell Signaling Technology). After washing with PBS, the resulting samples were stained with goat anti-rabbit immunoglobulin (IgG) [heavy and light chains (H + L)] secondary antibody or Alexa Fluor 546 (Invitrogen), goat anti-mouse IgG (H + L) secondary antibody, and Alexa Fluor 633 conjugate (Invitrogen) for 40 min at RT. Nuclei were labeled with

4′,6-diamidino-2-phenylindole (DAPI, Sigma-Aldrich), and F-actin was labeled with Alexa Fluor 546 phalloidin (Thermo Fisher Scientific) if necessary. All fluorescence images were taken using Prairie Technologies 2-photon and confocal microsope, QuantEM 512SC camera, 60× and 40× objective lenses, and native Prairie View software and visualized by z-stack mode. All the image analysis and processing were performed with ImageJ and Imaris.

Sectioning samples

After fixation, the hydrogels containing cells were embedded in optimal cutting temperature compound (OCT compound)-compound solution (Tissue-Tek) at −80°C for 30 min and sectioned to the thickness of 15 to 30 μm via a cryostat NX50 (Thermo Fisher Scientific). Sectioned samples were used to characterize β-catenin nuc/cyt ratio and measure actin intensity after immunostaining.

Blocking cell-ECM interactions

For blocking RGD-binding integrins, NSCs were preincubated for 30 min with 500 μg of RGD sequence–containing peptide (GRGDSP, Bachem) and control (GRADSP, Bachem) before encapsulation with hydrogel. After encapsulation, mixed differentiation media containing the peptides were added to each well. Optimal concentration of the peptides was determined by cell adhesion assay. The peptide-treated cells with varied peptide concentrations were seeded onto the RGD peptide–ligated (1 mM) HA-DBCO hydrogels (1 kPa). After 24 hours, the samples were washed twice with PBS, and the number of adhered cells was counted for each concentration condition. For inhibiting the protein secretion of cells, 150 μM 2-(4fluorobenzoylamino)-benzoic acid methyl ester (Exo-1; Sigma-Aldrich) dissolved in DMSO was used to treat the cells in mixed differentiation medium right after encapsulation. DMSO treatment was performed for control. The optimal concentration of Exo-1 was obtained by LIVE-DEAD assay with varied Exo-1 concentrations after 24 hours.

RNA isolation and qPCR

NSCs were extracted from HA-DBCO gels by incubating the gels in DMEM/F-12 containing hyaluronidase (750 to 3000 U/ml; Sigma-Aldrich) for 30 min at 37°C. The suspensions were centrifuged at 200*g* for 2 min to pellet cells and washed with PBS. Phenol-free total RNA was extracted from the cell pellets using RNeasy Plus Micro Kit with gDNA eliminator columns (Qiagen) following the manufacturer's protocol. After measurement of total RNA concentration, 600 ng of RNA was converted to cDNA using an iScript cDNA synthesis kit (Bio-Rad). Obtained cDNA was used for SYBR Green (Bimake) quantitative PCR (qPCR) with a 5 μM final forward and reverse primer concentration. Primer sequence was listed in table S1. qPCR was conducted for 34 cycles in a CFX Connect real-time PCR system (Bio-Rad). RNA level analysis was performed by the ddC_t method, and each gene expression was internally normalized by the expression level of housekeeping gene (S18) (*58*) run on the same qPCR batch.

RNA-seq and data analysis

RNA was isolated and purified as described above with two biological replicates per each hydrogel condition (RGD^-/soft, RGD^-/stiff, RGD^+/soft, and RGD^+/stiff). RNA integrity number (RIN) was assessed by using an Agilent 2100 Bioanalyzer (Agilent Technologies), and the high quality of RNA (RIN ≥ 9.8) was used. RNA-seq library preparation and batch-tag-RNA-seq (3′-tag-seq gene expression profiling) were carried out by the DNA Technologies and Expression Analysis Core at the University of California, Davis Genome Center. The reads were initially trimmed using BBDuk to remove Illumina adapters and to filter low-quality reads. The samples were then aligned to ratRibosomal genes using bbmap to remove ribosomal contaminated RNA. Any samples less than 21 bases were removed using BBDuk. Read quality analysis was performed using FastQC to assure that there was a Phred score >28. The reads were aligned to the *Rattus norvegicus* genome (rn6) using hisat2 v2.1.0. Then, the aligned reads were converted to counts using htseq. Normalization and differential expression analysis were conducted using DESeq2 and other Bioconductor packages in R. DEGs were determined with the condition of *P* value less than 0.05. Heatmaps and volcano plots were also obtained by Bioconductor packages in R.

Western blotting

NSCs embedded in HA-DBCO hydrogels were isolated by treating hyaluronidase (750 to 3000 U/ml; Sigma-Aldrich) at 37°C for 30 min as previously described above. Total protein was extracted from the cell pellet washed with PBS once by lysing with radioimmunoprecipitation assay lysis buffer (Sigma-Aldrich) containing Halt proteinase and phosphatase inhibitor cocktail (Thermo Fisher Scientific) on ice for 10 min. The protein concentration was determined by bicinchoninic acid (BCA) assay with Pierce BCA protein assay kit (Thermo Fisher Scientific), and samples were normalized with respect to protein content. Proteins were separated via SDS–polyacrylamide gel electrophoresis and transferred onto nitrocellulose membranes (0.22 μm; Odyssey). Membranes were blocked in a tris-buffered saline (TBS) blocking buffer (Odyssey) for 40 min and incubated with primary antibodies [rabbit anti-Egr1 (1:1000; Cell Signaling Technology), mouse anti-YAP (1:1000; Cell Signaling Technology), rabbit anti-Axin1 (1:1000; Invitrogen), and mouse anti–β-actin (1:10000; Sigma-Aldrich)] overnight at 4°C. Then, the membranes were washed with TBST and treated with biotinylated secondary antibodies [goat anti-rabbit IgG H + L (biotin) (1:10,000, Abcam) or goat anti-mouse IgG H + L (biotin) (1:10,000; Abcam)] and streptavidin-conjugated fluorescent label [Streptavidin, Alexa Fluor 790 conjugate (Invitrogen) or Streptavidin, Alexa Fluor 700 conjugate (Invitrogen)], sequentially. The membranes were washed with TBST and imaged by Odyssey CLx (LI-COR Biosciences).

shRNA cloning

shRNA inserts were designed with Age I– and Eco RI–based overhangs using Ensembl genome browser and the online tool, InvivoGen. shRNA targeting rat Egr1 (shEGR1-1, GCCGAGATGCAATTGATGTCT; shEGR1-2, GTCGAATCTGCATGCGTAATT) and a scramble control (GTCGGCTACGAAGGTATTCTA) were obtained from Elim Biopharmaceuticals. The inserts were ligated into the pLKO.1 puro vector (plasmid no. 10878, Addgene).

Viral packaging and transduction

Lentiviral particles were packaged in human embryonic kidney (HEK) 293 T cells with psPAX2 and pMD2.G through polyethylenimine (PEI) transfection and purified as previously described (*59*). Purified viral particles were transduced to the NSCs with a multiplicity of infection (MOI) of 1, and shRNA-expressing cells were selected using puromycin (1 μg/ml) longer than 4 days. Retroviral vectors were packaged in HEK 293 T cells with Gag/pol and VSV-G through PEI

transfection with plasmids for *Egr1* overexpression (pMXs-hs-EGR1, plasmid no. 52724, Addgene) and control (pMXs-puro GFP-p62, plasmid no. 38277, Addgene). NSCs were infected with the resulting vectors at an approximate MOI of 1 (titering of the virus was carried out with pMXs-puro GFP-p62 by puro-based selection).

Nuclear to cytoplasmic ratio quantification

Images from 30-μm sectioned samples costained for total β-catenin and total YAP, nuclear staining, and F-actin staining were used to quantify β-catenin and YAP nuclear-to-cytosolic ratio based on fluorescence intensity. Binary masks of the nuclei and actin were obtained from DAPI and phalloidin images and superimposed each other to create masks that contain the cytosol but exclude the nucleus. Then, the total β-catenin fluorescence intensity was quantified in these regions, and their ratio was calculated followed by normalizing to the area of each domain

$$\beta - \text{Catenin}\,\frac{\text{nuc}}{\text{cyt}}\,\text{ratio} = \frac{\dfrac{\text{integrated intensity of nuclear } \beta - \text{catenin}}{\text{area of nucleus}}}{\dfrac{\text{integrated intensity of cytosolic } \beta - \text{catenin}}{\text{area of cytosol}}}$$

Luciferase assay

Naïve NSCs and Egr1 KD NSC cell lines were transduced with a lentiviral construct encoding a 7xTFP T cell factor/lymphoid enhancer factor (TCF/LEF) luciferase reporter, which represents β-catenin–TCF/LEF–based transcription. Cell pellets from the cells encapsulated with HA-DBCO gel under each condition were obtained after 3 days of encapsulation/differentiation as described above. The cell pellets were washed with PBS once, lysed with lysis buffer (Promega), and centrifuged to pellet debris. Suspensions were loaded to each well of a white opaque 96-well plate, and Luciferase Assay Reagent (Promega) was treated right before detection. Luminescence intensity was detected via SpectraMax luminometer (Molecular Devices) and normalized to total protein concentration obtained through BCA protein assay (Pierce) to consider the variation of proliferation between samples.

Image analysis

Actin intensity was quantified by extraction of intensity line scans perpendicular to the membrane by linearizing of the cell edges using Fiji. Rhodamine phalloidin–stained fluorescence images for the cells encapsulated within 3D gels for 5 hours after gel sectioning were used for the analysis. Obtained intensity line scans were fitted, and then the peak intensity was measured through Origin data analysis software to quantify actin intensity. Full width at half maximum of the Gaussian whose peak was located closest to the center of the line was used as a measure of thickness by Origin. Cellular volume was measured by using Imaris 3D imaging software. Fluorescence images showing 3D rendering of single NSCs stained with cell membrane dye (R18) were used to quantify the volume.

ABAQUS simulation

To analyze the stress distribution of the hydrogel with the growth of the cell, the finite element analysis was conducted using a nonlinear static solver in ABAQUS 6.14. The sphere-shaped cell and the hexahedron-shaped hydrogel were modeled as a 3D deformable solid, and the cell was designed to be located at the center of the hydrogel. The experimentally obtained cellular volume was used as cell sizes, and the length of each side of the hydrogel was assumed as 100 μm. The element type of the cell and the hydrogel was a C3D20R (a 20-node quadratic brick, reduced integration). The elastic modulus of the hydrogel, assumed to be isotropic, was obtained with its shear modulus and Poisson's ratio: $E = 2G(1 + \nu)$. For the calculation, the shear modulus values of each hydrogel obtained by rheometer were used, and the Poisson's ratio was assumed to be 0.49. Meanwhile, the elastic modulus and Poisson's ratio of the cell were designated to have constant values of 500 Pa and 0.49, respectively.

Inhibition experiments

To inhibit myosin II, FAK, and actin assembly, NSCs were preincubated with blebbistatin (1 μM; Sigma-Aldrich), PF-573228 (0.5 μM, Sigma-Aldrich), and cyt D (1 μM, Sigma-Aldrich), respectively, for 20 min. Right after gelation, these were added to the media with the same concentration under the spontaneous differentiation condition. Then, the cells were harvested after 5 hours to investigate whether each inhibition affect *Egr1* mRNA expression. JIB-04 (3 μM; Cayman Chemical Company), pan-selective Jumonji histone demethylase inhibitor, was treated to cell media right after encapsulation of NSCs with 3D gels to see the effect of H3K9me3 on *Egr1* expression.

H3K9me3 quantification

Histone lysates were isolated from the cells (1×10^6) incubated within each hydrogel for 3 hours under differentiation condition by Epiquik Total Histone Extraction Kit (Epigentek), and the quantification of H3K9me3 level was performed with EpiQuik Global Tri-Methyl Histone H3K9 Quantification Kit (Epigentek) following the protocols provided by the manufacturer.

Statistical analysis

All the quantitative data were presented as the means ± SD, and the number of biological and technical replicates is indicated in the figure legends and Materials and Methods. One-way analysis of variance (ANOVA) followed by Tukey test and Student's *t* test for between-group differences were performed with GraphPad Prism as indicated in the figure legends.

SUPPLEMENTARY MATERIALS

Supplementary material for this article is available at https://science.org/doi/10.1126/sciadv.abm4646

View/request a protocol for this paper from *Bio-protocol*.

REFERENCES AND NOTES

1. W. L. Murphy, T. C. McDevitt, A. J. Engler, Materials as stem cell regulators. *Nat. Mater.* **13**, 547–557 (2014).
2. A. J. Engler, S. Sen, L. H. Sweeney, D. E. Discher, Matrix elasticity directs stem cell lineage specification. *Cell* **126**, 677–689 (2006).
3. S. B. Han, J. K. Kim, G. Lee, D. H. Kim, Mechanical properties of materials for stem cell differentiation. *Adv. Biosys.* **4**, 2000247 (2020).
4. K. H. Vining, D. J. Mooney, Mechanical forces direct stem cell behaviour in development and regeneration. *Nat. Rev. Mol. Cell Biol.* **18**, 728–742 (2017).
5. N. Huebsch, P. R. Arany, A. S. Mao, D. Shvartsman, O. A. Ali, S. A. Bencherif, J. Rivera-Feliciano, D. J. Mooney, Harnessing traction-mediated manipulation of the cell/matrix interface to control stem-cell fate. *Nat. Mater.* **9**, 518–526 (2010).
6. Y. Sun, K. Yong, L. G. Villa-Diaz, X. Zhang, W. Chen, R. Philson, S. Weng, H. Xu, P. H. Krebsbach, J. Fu, Hippo/YAP-mediated rigidity-dependent motor neuron differentiation of human pluripotent stem cells. *Nat. Mater.* **13**, 599–604 (2014).
7. C. Argentati, F. Morena, I. Tortorella, M. Bazzucchi, S. Porcellati, C. Emiliani, S. Martino, Insight into Mechanobiology: How stem cells feel mechanical forces and orchestrate biological functions. *Int. J. Mol. Sci.* **20**, 5337 (2019).
8. W. J. Hadden, J. L. Young, A. W. Holle, M. L. McFetridge, D. Kim, P. Wijesinghe, H. Taylor-Weiner, J. H. Wen, A. R. Lee, K. Bieback, B.-N. Vo, D. D. Sampson, B. F. Kennedy,

J. P. Spatz, A. J. Engler, Y. Choi, Stem cell migration and mechanotransduction on linear stiffness gradient hydrogels. *Proc. Natl. Acad. Sci. U.S.A.* **114**, 5647–5652 (2017).
9. A. J. Keung, E. M. de Juan-Pardo, D. V. Schaffer, S. Kumar, Rho GTPases mediate the mechanosensitive lineage commitment of neural stem cells. *Stem Cells* **29**, 1886–1897 (2011).
10. S. Rammensee, M. S. Kang, K. Georgiou, S. Kumar, D. V. Schaffer, Dynamics of mechanosensitive neural stem cell differentiation. *Stem Cells* **35**, 497–506 (2017).
11. B. M. Baker, C. S. Chen, Deconstructing the third dimension – how 3D culture microenvironments alter cellular cues. *J. Cell Sci.* **125**, 3015–3024 (2012).
12. M. Bao, J. Xie, W. T. S. Huck, Recent advances in engineering the stem cell microniche in 3D. *Adv. Sci.* **5**, 1800448 (2018).
13. T. Iskratsch, H. Wolfenson, M. P. Sheetz, Appreciating force and shape — the rise of mechanotransduction in cell biology. *Nat. Rev. Mol. Cell Biol.* **15**, 825–833 (2014).
14. K. A. Jansen, P. Atherton, C. Ballestrem, Mechanotransduction at the cell-matrix interface. *Semin. Cell Dev. Biol.* **71**, 75–83 (2017).
15. J. Huang, L. Wang, C. Xiong, F. Yuan, Elastic hydrogel as a sensor for detection of mechanical stress generated by single cells grown in three-dimensional environment. *Biomaterials* **98**, 103–112 (2016).
16. O. Chaudhuri, L. Gu, D. Klumpers, M. Darnell, S. A. Bencherif, J. C. Weaver, N. Huebsch, H.-p. Lee, E. Lippens, G. N. Duda, D. J. Mooney, Hydrogels with tunable stress relaxation regulate stem cell fate and activity. *Nat. Mater.* **15**, 326–334 (2016).
17. D. J. Mooney, H.-p. Lee, L. Gu, M. E. Levenston, O. Chaudhuri, Mechanical confinement regulates cartilage matrix formation by chondrocytes. *Nat. Mater.* **16**, 1243–1251 (2017).
18. S. Khetan, M. Guvendiren, W. R. Legant, D. M. Cohen, C. S. Chen, J. A. Burdick, Degradation-mediated cellular traction directs stem cell fate in covalently crosslinked three-dimensional hydrogels. *Nat. Mater.* **12**, 458–465 (2013).
19. S. R. Caliari, S. L. Vega, M. Kwon, E. M. Soulas, J. A. Burdick, Dimensionality and spreading influence MSC YAP/TAZ signaling in hydrogel environments. *Biomaterials* **103**, 314–323 (2016).
20. C. M. Madl, B. L. LeSavage, R. E. Dewi, C. B. Dinh, R. S. Stowers, M. Khariton, K. J. Lampe, D. Nguyen, O. Chaudhuri, A. Enejder, S. C. Heilshorn, Maintenance of neural progenitor cell stemness in 3D hydrogels requires matrix remodelling. *Nat. Mater.* **16**, 1233–1242 (2017).
21. M. Bergert, A. Erzberger, R. A. Desai, I. M. Aspalter, A. C. Oates, G. Charras, G. Salbreux, E. K. Paluch, Force transmission during adhesion-independent migration. *Nat. Cell Biol.* **17**, 524–529 (2015).
22. K. M. Stroka, H. Jiang, S.-H. Chen, Z. Tong, D. Wirtz, S. X. Sun, K. Konstantopoulos, Water permeation drives tumor cell migration in confined microenvironments. *Cell* **157**, 611–623 (2014).
23. M. M. Adil, T. Vazin, B. Ananthanarayanan, G. Rodrigues, A. T. Rao, R. U. Kulkarni, E. W. Miller, S. Kumar, D. V. Schaffer, Engineered hydrogels increase the post-transplantation survival of encapsulated hESC-derived midbrain dopaminergic neurons. *Biomaterials* **136**, 1–11 (2017).
24. B. S. Elkin, E. U. Azeloglu, K. D. Costa, B. Morrison, Mechanical heterogeneity of the rat hippocampus measured by atomic force microscope indentation. *J. Neurotrauma* **24**, 812–822 (2007).
25. I. Sack, B. Beierbach, U. Hamhaber, D. Klatt, J. Braun, Non-invasive measurement of brain viscoelasticity using magnetic resonance elastography. *NMR Biomed.* **21**, 265–271 (2008).
26. I. Levental, P. C. Georges, P. A. Janmey, Soft biological materials and their impact on cell function. *Soft Matter* **3**, 299–306 (2007).
27. M. Zhang, Y. Liao, B. Lönnerdal, EGR-1 is an active transcription factor in TGF-β2-mediated small intestinal cell differentiation. *J. Nutr. Biochem.* **37**, 101–108 (2016).
28. J. Sun, J. Chen, E. Mohagheghian, N. Wang, Force-induced gene up-regulation does not follow the weak power law but depends on H3K9 demethylation. *Sci. Adv.* **6**, eaay9095 (2020).
29. F. Duclot, M. Kabbaj, The role of early growth response 1 (EGR1) in brain plasticity and neuropsychiatric disorders. *Front. Behav. Neurosci.* **11**, 35 (2017).
30. Y. Feng, S. Yu, T. K. R. Lasell, A. P. Jadhav, E. Macia, P. Chardin, P. Melancon, M. Roth, T. Mitchison, T. Kirchhausen, Exo1: A new chemical inhibitor of the exocytic pathway. *Proc. Natl. Acad. Sci.* **100**, 6469–6474 (2003).
31. R. H. Bonow, S. Aïd, Y. Zhang, K. G. Becker, F. Bosetti, The brain expression of genes involved in inflammatory response, the ribosome, and learning and memory is altered by centrally injected lipopolysaccharide in mice. *Pharmacogenomics J.* **9**, 116–126 (2009).
32. A. Veyrac, A. Gros, E. Bruel-Jungerman, C. Rochefort, F. B. Borgmann, S. Jessberger, S. Laroche, Zif268/egr1 gene controls the selection, maturation and functional integration of adult hippocampal newborn neurons by learning. *Proc. Natl. Acad. Sci. U.S.A.* **110**, 7062–7067 (2013).
33. M. Mullin, K. Lightfoot, R. Clarke, M. Miller, R. Lahesmaa, D. Cantrell, The RhoA transcriptional program in pre-T cells. *FEBS Lett.* **581**, 4309–4317 (2007).
34. S. Davis, P. Vanhoutte, C. Pagès, J. Caboche, S. Laroche, The MAPK/ERK cascade targets both Elk-1 and cAMP response element-binding protein to control long-term potentiation-dependent gene expression in the dentate gyrus in vivo. *J. Neurosci.* **20**, 4563–4572 (2000).
35. D.-C. Lie, S. A. Colamarino, H.-J. Song, L. Désiré, H. Mira, A. Consiglio, E. S. Lein, S. Jessberger, H. Lansford, A. R. Dearie, F. H. Gage, Wnt signalling regulates adult hippocampal neurogenesis. *Nature* **437**, 1370–1375 (2005).
36. L. Zhang, X. Yang, S. Yang, J. Zhang, The Wnt/β-catenin signaling pathway in the adult neurogenesis. *Eur. J. Neurosci.* **33**, 1–8 (2011).
37. J. Otero, W. Fu, L. Kan, A. E. Cuadra, J. A. Kessler, β-Catenin signaling is required for neural differentiation of embryonic stem cells. *Development* **131**, 3545–3557 (2004).
38. R. S. Ashton, A. Conway, C. Pangarkar, J. Bergen, K.-I. Lim, P. Shah, M. Bissell, D. V. Schaffer, Astrocytes regulate adult hippocampal neurogenesis through ephrin-B signaling. *Nat. Neurosci.* **15**, 1399–1406 (2012).
39. C. Fuerer, R. Nusse, Lentiviral vectors to probe and manipulate the wnt signaling pathway. *PLOS ONE* **5**, e9370 (2010).
40. G. Brusatin, T. Panciera, A. Gandin, A. Citron, S. Piccolo, Biomaterials and engineered microenvironments to control YAP/TAZ-dependent cell behaviour. *Nat. Mater.* **17**, 1063–1075 (2018).
41. S. Dupont, L. Morsut, M. Aragona, E. Enzo, S. Giulitti, M. Cordenonsi, F. Zanconato, J. Digabel, M. Forcato, S. Bicciato, N. Elvassore, S. Piccolo, Role of YAP/TAZ in mechanotransduction. *Nature* **474**, 179–183 (2011).
42. J. Baek, S.-Y. Cho, H. Kang, H. Ahn, W.-B. Jung, Y. Cho, E. Lee, S.-W. Cho, H.-T. Jung, S. Im, Distinct mechanosensing of human neural stem cells on extremely-limited anisotropic cellular contact. *ACS Appl. Mater. Interfaces* **10**, 33891–33900 (2018).
43. E. Cognard, C. G. Dargaville, D. L. Hay, P. R. Shepherd, Identification of a pathway by which glucose regulates β-catenin signalling via the cAMP/protein kinase A pathway in β-cell models. *Biochem. J.* **449**, 803–811 (2013).
44. S. Taurin, N. Sandbo, Y. Qin, D. Browning, N. O. Dulin, Phosphorylation of β-catenin by cyclic AMP-dependent protein kinase*. *J. Biol. Chem.* **281**, 9971–9976 (2006).
45. M. Zhang, E. Mahoney, T. Zuo, P. K. Manchanda, R. V. Davuluri, L. S. Kirschner, Protein kinase A activation enhances β-catenin transcriptional activity through nuclear localization to PML bodies. *PLOS ONE* **9**, e109523 (2014).
46. G. Zhu, Y. Wang, B. Huang, J. Liang, Y. Ding, A. Xu, W. Wu, A Rac1/PAK1 cascade controls β-catenin activation in colon cancer cells. *Oncogene* **31**, 1001–1012 (2012).
47. R. McBeath, D. M. Pirone, C. M. Nelson, K. Bhadriraju, C. S. Chen, Cell shape, cytoskeletal tension, and RhoA regulate stem cell lineage commitment. *Dev. Cell* **6**, 483–495 (2004).
48. A. Hall, Rho GTPases and the actin cytoskeleton. *Science* **279**, 509–514 (1998).
49. C. Cadart, L. Venkova, P. Recho, M. Lagomarsino, M. Piel, The physics of cell-size regulation across timescales. *Nat. Phys.* **15**, 993–1004 (2019).
50. J. Chen, B. Ananthanarayanan, K. S. Springer, K. J. Wolf, S. M. Sheyman, V. D. Tran, S. Kumar, Suppression of LIM kinase 1 and LIM kinase 2 limits glioblastoma invasion. *Cancer Res.* **80**, 69–78 (2020).
51. R. S. Stowers, A. Shcherbina, J. Israeli, J. J. Gruber, J. Chang, S. Nam, A. Rabiee, M. N. Teruel, M. P. Snyder, A. Kundaje, O. Chaudhuri, Matrix stiffness induces a tumorigenic phenotype in mammary epithelium through changes in chromatin accessibility. *Nat. Biomed. Eng.* **3**, 1009–1019 (2019).
52. A. Belyaeva, S. Venkatachalapathy, M. Nagarajan, G. V. Shivashankar, C. Uhler, Network analysis identifies chromosome intermingling regions as regulatory hotspots for transcription. *Proc. Natl. Acad. Sci.* **114**, 13714–13719 (2017).
53. R. T. Moon, A. D. Kohn, G. V. Ferrari, A. Kaykas, WNT and β-catenin signalling: Diseases and therapies. *Nat. Rev. Genet.* **5**, 691–701 (2004).
54. M. J. Perugorria, P. Olaizola, I. Labiano, A. Esparza-Baquer, M. Marzioni, J. J. G. Marin, L. Bujanda, J. M. Banales, Wnt–β-catenin signalling in liver development, health and disease. *Nat. Rev. Gastroenterol. Hepatol.* **16**, 121–136 (2019).
55. S. A. Ferreira, M. S. Motwani, P. A. Faull, A. J. Seymour, T. T. L. Yu, M. Enayati, D. K. Taheem, C. Salzlechner, T. Haghighi, E. M. Kania, O. P. Oommen, T. Ahmed, S. Loaiza, K. Parzych, F. Dazzi, O. P. Varghese, F. Festy, A. E. Grigoriadis, H. W. Auner, A. P. Snijders, L. Bozec, E. Gentleman, Bi-directional cell-pericellular matrix interactions direct stem cell fate. *Nat. Commun.* **9**, 4049 (2018).
56. C. Loebel, R. L. Mauck, J. A. Burdick, Local nascent protein deposition and remodelling guide mesenchymal stromal cell mechanosensing and fate in three-dimensional hydrogels. *Nat. Mater.* **18**, 883–891 (2019).
57. T. D. Palmer, E. A. Markakis, A. R. Willhoite, F. Safar, F. H. Gage, Fibroblast growth factor-2 activates a latent neurogenic program in neural stem cells from diverse regions of the adult CNS. *J. Neurosci.* **19**, 8487–8497 (1999).
58. J. Peltier, S. Agrawal, M. J. Robertson, D. V. Schaffer, Protocols for adult stem cells. *Methods Mol. Biol.* **621**, 65–87 (2010).
59. J. Peltier, D. V. Schaffer, Protocols for adult stem cells. *Methods Mol. Biol.* **621**, 103–116 (2010).

Acknowledgments: We thank O. Teter (UC Berkeley–UC San Francisco Graduate Program in Bioengineering) for experimental assistance. **Funding:** This work was supported by the NIH (R01NS074831 to S.K. and D.V.S.), a Siebel Fellowship to J.B., and a Graduate Research

Fellowship (National Science Foundation) to P.A.L. RNA-seq was carried by the DNA Technologies and Expression Analysis Core at the UC Davis Genome Center, supported by the NIH Shared Instrumentation grant 1S10OD010786-01. **Author contributions:** J.B. designed and performed the experiments, analyzed and interpreted the data, and wrote the manuscript. P.A.L. contributed to RNA-seq analysis and the experiment for generating *Egr1* KD cells. S.L. and T.-S.K. conducted ABAQUS simulation. S.K. and D.V.S. supervised the project, helped in the experimental design and data interpretation, and cowrote the manuscript. **Competing interests:** The authors declare that they have no competing interests. **Data and materials availability:** All data needed to evaluate the conclusions in the paper are present in the paper and/or the Supplementary Materials. The RNA-seq data discussed in this manuscript have been deposited in the National Center for Biotechnology Information's Gene Expression Omnibus (GEO) and are accessible through GEO Series accession number GSE193194: www.ncbi.nlm.nih.gov/geo/query/acc.cgi?acc=GSE193194

Submitted 20 September 2021
Accepted 28 February 2022
Published 15 April 2022
10.1126/sciadv.abm4646

ScienceAdvances

Egr1 is a 3D matrix–specific mediator of mechanosensitive stem cell lineage commitment

Jieung BaekPaola A. LopezSangmin LeeTaek-Soo KimSanjay KumarDavid V. Schaffer

Sci. Adv., 8 (15), eabm4646. • DOI: 10.1126/sciadv.abm4646

Science Advances (ISSN) is published by the American Association for the Advancement of Science. 1200 New York Avenue NW, Washington, DC 20005. The title *Science Advances* is a registered trademark of AAAS.